water

MDPI

Article

Experimental Assessment of a New Kinetic Turbine Performance for Artificial Channels

Cécile Münch-Alligné [1,*], Jérémy Schmid [1], Sylvain Richard [1], Anthony Gaspoz [1], Nino Brunner [2] and Vlad Hasmatuchi [1]

1 Systems Engineering Institute, School of Engineering, University of Applied Sciences and Arts Western Switzerland, Route du Rawyl 47, 1950 Sion, Switzerland; jeremy.schmid@hevs.ch (J.S.); sylvain.richard@hevs.ch (S.R.); anthony.gaspoz@hevs.ch (A.G.); vlad.hasmatuchi@hevs.ch (V.H.)

2 Stahleinbau GmBH, Talstrasse 30, 3922 Stalden, Switzerland; brunner.nino@stahleinbau.ch

* Correspondence: cecile.muench@hevs.ch; Tel.: +41-27-606-88-39

Received: 22 December 2017; Accepted: 9 March 2018; Published: 13 March 2018

Abstract: An experimental investigation to measure the performance of a first prototype of a kinetic turbine is presented. This turbine, developed using numerical simulation, recovers the kinetic energy of water in free surface canals. To assess the performance of the machine, a first prototype as well as an open-air platform were built, both installed in the tailrace canal of Lavey hydropower plant. This is the first time in Switzerland that on-site experiments have been carried out for kinetic turbines. An experimental procedure was set up using measurements in the laboratory and on site to assess the power coefficient of the turbine as a function of the tip speed ratio. The influence of the turbine depth and the tilt of the turbine axis were also explored. A maximal power coefficient of 0.93 was reached for the higher tilt and depth investigated.

Keywords: kinetic turbine; small hydro; pilot site; experimental performance measurements

1. Introduction

To tap the renewable potential of ocean and river streams, new hydraulic machines have been developed over several decades. Contrary to standard hydraulic energy conversion machines, this type of turbines mostly harnesses the kinetic energy of water or possibly a very low head; those machines are classified as low pressure technology, under 2.4 m head [1]. In 2009, Kahn et al. [2] performed a large review of the different technologies and research projects on this type of conversion system. Most of these technologies are still at the demonstration stage in operational environment [2,3]. Only a few MWh are injected into the grid despite the fact that large technically recoverable potentials of 800 TWh per year are commonly assessed for tidal energy in the world and 120 TWh per year for river energy in the US [3].

A variety of solutions are under development to harvest the kinetic energy of water, namely, turbine and non-turbine systems. Concerning turbine technologies, their name differs according to application; for ocean, the generic terms are "water current turbine" or "tidal current turbine"; for river or artificial canal, "river turbine" or "kinetic turbine" are preferred. The last term will be used in this paper. Indeed, the applications targeted here are artificial water canals or river streams, covered by [4,5] in Canada or [6] in France.

For both applications, the turbine can be ducted or in a free-stream, and the rotational axis can be horizontal or vertical [2]. In the case of free stream turbines, the power coefficient is limited by the well-known Betz's theory [7], and equal to 16/27. The improvement of the power density using a Venturi duct to accelerate the flow through the runner, and has been proved by several studies for wind and water applications [8,9]. According to Kirke [9], the theoretical limit for a diffuser-augmented wind turbine can reach about 3.3 times the Betz limit and a model diffuser augmented wind turbine has

extracted 4.25 times the power extracted by the same turbine without a diffuser. To identify the optimal couple "diffuser-runner", an optimal range for the turbine resistance coefficient was identified [10]. This optimization can be performed using numerical simulations [11,12].

The turbine studied here presents a horizontal axis with a Venturi duct. This research project is the first one in Switzerland including an on-site demonstration phase, where small hydro represents 50% of the remaining hydraulic potential—estimated between 1300 and 1600 GWh [13]. Today, small hydropower represents 5% of the electricity production with more than 1000 plants producing each year 3400 GWh [14]. Part of the potential is located in existing infrastructure such as drinking water networks [15] or tailrace canals of large hydropower plants [16]. To harvest this potential, new technologies should be developed to ensure robustness, low CAPEX, and reliability.

The aim of the research project is to set up a newly-ducted horizontal axis turbine. Numerical simulations were used to simplify as much as possible the design to reach an economic feasibility, since the power density of this type of turbine is low. To assess the performance of the turbine, a first prototype was built as well as an open-air platform. Both were installed in 2017 on a pilot site, identified quite early in the project, and characterized using both experimental measurements and numerical simulations [16,17].

In this paper, the concept of this kinetic turbine of 1 kW and the technical sizing are first presented. Then, the experimental setup as well as the pilot site are described. The experimental measurements on site are carried out including the investigation of the influence of two main parameters: the depth and the tilt of the turbine axis.

2. The Kinetic Turbine Concept and Its Open-Air Platform

The hydraulic concept of the turbine is characterized by a horizontal rotational shaft and a Venturi duct. This duct is composed of four parts, respectively: a straight inlet section, a convergent part, a straight part for the runner, and an outlet diffuser. The final geometry of the duct has an inlet diameter of 1.128 m and an outlet diameter of 1.60 m, its total length being more than 4 m in Figure 1.

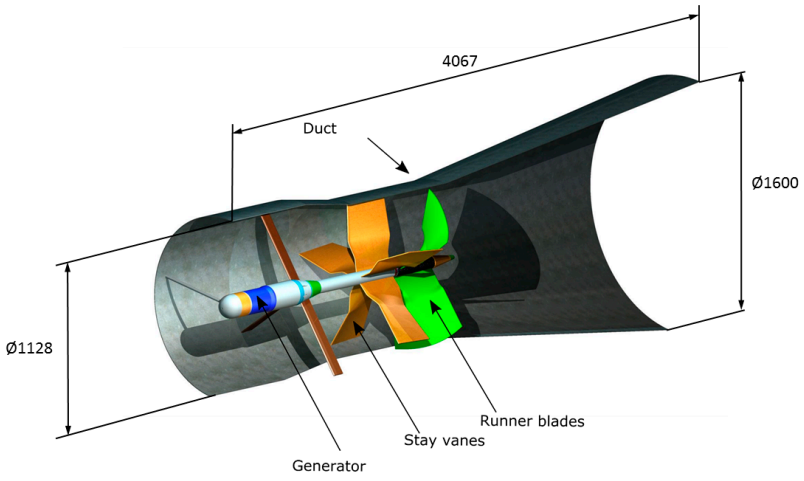

Figure 1. Sketch of the kinetic turbine prototype along with main characteristic lengths (lenghts in mm).

The role of this turbine component is to increase the flow velocity across the runner by increasing the harnessed upstream flow. Five stay vanes support the duct and guide the flow in the runner. The runner, composed of three fixed blades, has a diameter of 1 m. This part of the turbine plays a major role in transferring the hydraulic energy into mechanical energy by rotating the central horizontal shaft. The runner recovers the torque all along the blades. Alternative technologies propose a pump design in the center [18] or only an annular runner [19] to increase the Venturi effect. Close to the hub,

the runner blade allows a diminution of the blockage effect to let the flow accelerate in this region while in the peripheral part, the maximum of the torque is recovered, see Figure 2.

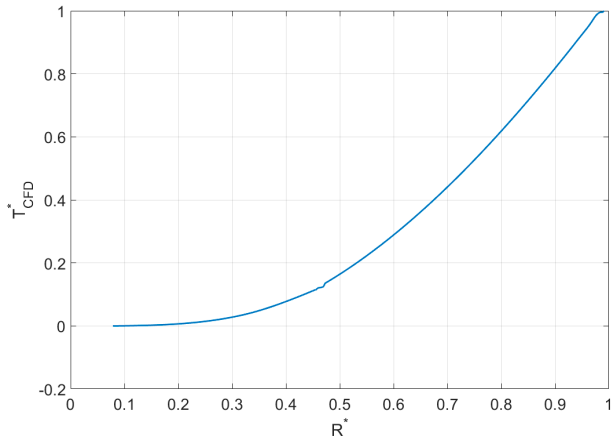

Figure 2. Cumulated normalized torque along the blade for nominal conditions from CFD, extracted from previous simulations, [16].

The shaft of the turbine includes an inlet bulb section where the generator is placed along with the mechanical elements, allowing the transformation of the mechanical energy into electricity; see Figure 1. The different components of the turbine have then been built by Stahleinbau GmBH mainly in stainless steel except the runner, which is made in cast aluminum.

A planetary gearbox was set between the runner and the generator to ensure a higher rotational speed of the generator and consequently a lower torque, with a factor of 16 being reached. A self-lubricating bearing is used to minimize the mechanical friction losses on the shaft on the runner side. The static water sealing is ensured with standard O-rings and a specific silicium carbide dynamic sealing for between the shaft and the casing. This protects the inner mechanical components against corrosion and scuffing while minimizing the friction.

The selected generator is a synchronous machine with permanent magnets composed of six pairs of poles, with a maximal power of 4.2 kW for a rotational speed of 2000 min^{-1}. This rotational speed is high enough to minimize the size of the electrical generator, which must be installed in the bulb of the machine. Since the nominal rotational speed of the turbine runner is much lower, the gearbox mentioned above ensures the necessary rotational speed multiplication ratio.

The rotational speed represents the degree of freedom of the machine to follow the variation of the upstream flow velocity and to investigate its whole operating range. Indeed, a nominal rotational speed was fixed during the design phase but a power electronics stage allows varying this parameter between 200 and 2000 min^{-1} at the generator side.

The performance of the turbine can be described by the power coefficient of the kinetic turbine, (see Equation (1)); as a function of the tip speed ratio, (see Equation (2)).

$$C_p = \frac{P_m}{P_h} = \frac{T_r \cdot \omega_r}{\frac{1}{2}\rho C_\infty^3 \pi R_r^2} = \frac{2\pi}{60}\frac{T_r \cdot N_r}{\frac{1}{2}\rho C_\infty^3 \pi R_r^2} \quad (1)$$

$$\lambda = \frac{\omega_r \cdot R_r}{C_\infty} = \frac{2\pi}{60}\frac{N_r \cdot R_r}{C_\infty} \quad (2)$$

The power coefficient of the turbine is based on the runner area as performed in other studies of ducted turbines such as Lawn [10]. This normalization allows to compare the value with the Betz limit. Using the inlet section, this power coefficient would be reduced by a factor of 0.79, whereas using the outlet section would produce a factor of 0.39.

The nominal operating condition of the turbine is fixed for an upstream velocity of 1.47 m·s^{-1} and the full load condition is expected for a velocity of 1.7 m·s^{-1}; see Table 1. Assuming a power coefficient of 0.85 and an efficiency of 0.7 for transmission between the mechanical power and the electrical power at the outlet of the generator, the target value for the maximal electrical power is 1148 kW.

Table 1. Nominal and full-load expected turbine characteristics.

Expected Turbine Characteristics		
	Full-load	Nominal
C_∞	1.7 m·s^{-1}	1.47 m·s^{-1}
P_h	1′930 W	1′247 W
λ		2.65
C_p		0.85
P_{mec}	1′640 W	1′060 W
N_r	86 min^{-1}	74.4 min^{-1}
N_g	1′376 min^{-1}	1′190 min^{-1}
P_{elec}	1′148 W	742 W

To assess the performance of this prototype, a specific open-air platform was set up. The open-air platform was designed to allow positioning the turbine at different depths and tilt angles in the canal. Moreover, it will support the researchers during the measurements. The platform is 14 m high, while the metal footbridge has a section of 5 m × 7.26 m. In the center of this footbridge, the kinetic turbine can be moved from the maximum level, where maintenance can be done, to the bottom of the tailrace canal along the two slice rods. The tilt angle, defined in Figure 3, can be modified as well. The adjustable tripodal base allows ensuring a vertical position for the rods and a horizontal orientation for the footbridge. The platform and the turbine have a total weight of 11 metric tons.

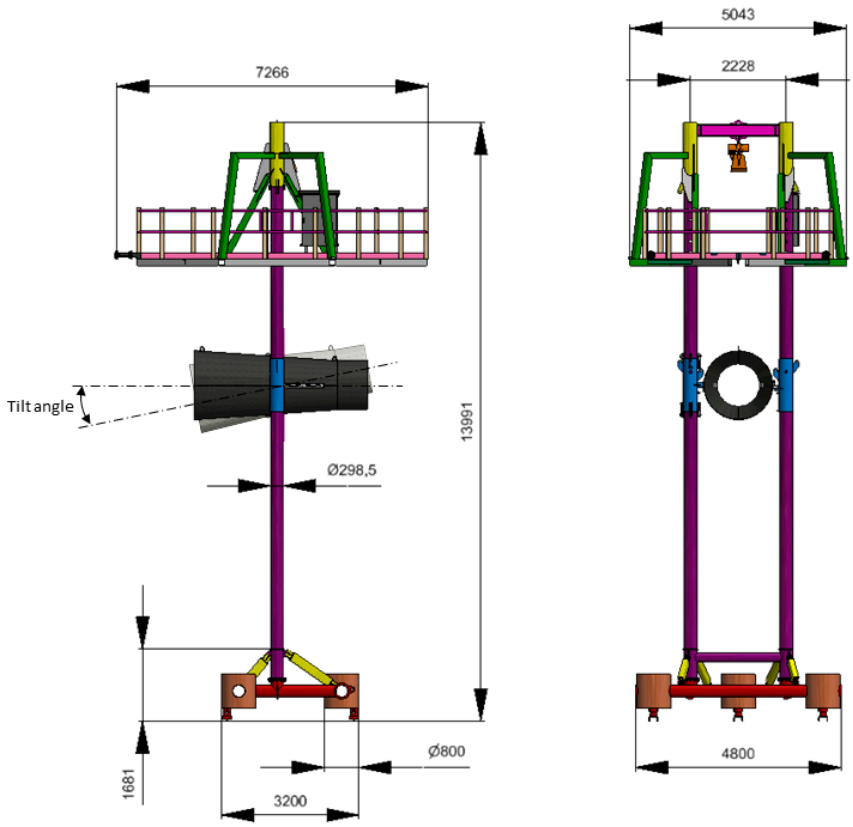

Figure 3. Description of the open-air platform developed for on-site measurements. (Lengths in mm).

3. Experimental Setup

3.1. Global Methodology

The experimental approach to assess the power coefficient C_p of the turbine as a function of the tip speed ratio λ is to measure some variables on site and to identify others in the laboratory in Figure 4.

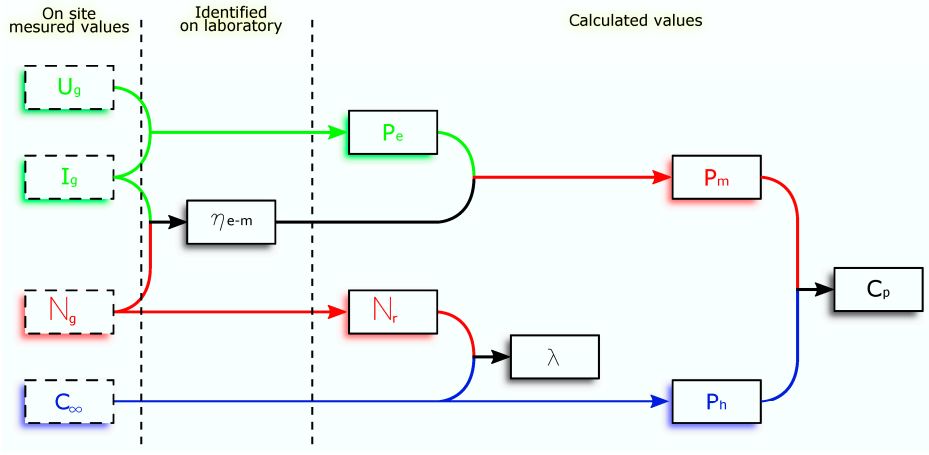

Figure 4. Experimental strategy to assess the performance of the turbine.

The characteristics of the main instruments used to measure the different quantities described in Figure 4 are provided in Table 2.

Table 2. Characteristics of the main measurement instruments.

Measured Quantity	Sensor Type	Range	Accuracy
Reference velocity (C_∞)	Teledyne Workhorse 1200 kHz ADCP system	±5 [m/s]	±0.3 [%] of water velocity relative to ADCP
Electrical power (P_e)	Zimmer LMG670 precision electrical multimeter	0.1000 [Vtrms] 0.32 [Atrms]	±0.015 [%]
Mechanical torque (T_r)	NCTE 3000 torquemeter	±250 [Nm]	±0.02 [%]
Current (I_g)	LEM IT 60-S ULTRASTAB current transducer	60 [Atrms]	±0.02725 [%]
Voltage (U_g)	LEM CV 3-1000 voltage transducer	1000 [Vtrms]	±0.2 [%]
Rotational speed (N_g)	Heidenhain ECN 1325 encoder	0.12000 [min^{-1}]	2048 [ppr]
Water depth	Endress&Hauser Cerabat T PMC131 relative pressure sensor	0.2 [bar]	±0.5 [%]
Water temperature	Endress&Hauser Easytemp TMR31 sensor	0.100 [°C]	±0.1 [%]
Tilt	DIS Sensors QG40N-KAXYZ-12,0-AI-PT 3-axis acceleration sensor	±12 [g]	±0.12 [g]
Data acquisition and control			
Teledyne RD Instruments ADCP system		- Dedicated to the values of the reference velocity	
NI CompactRIO 9035 controller		- Dedicated to the values of the prototype	

3.2. Identification of Variables in Laboratory

Before measuring on site, investigations were performed in the laboratory to identify the electro-mechanical efficiency η_{e-m} of the device as a function of the rotational speed of the generator N_g and the current at the terminals of the generator I_g.

The selected generator is a Phase TK142-100-041-G-R0-pa with permanent magnets composed of six pairs of poles, with a rated power of 2.39 kW and with a current of 6 A for a rotational speed of 1000 min^{-1}. The speed of the generator can reach a maximal value of 2000 rpm. The target operating conditions, corresponding to the turbine nominal conditions, are a power of 742 W for a rotational

speed of 1190 min^{-1}. As explained in Section 2, this rotational speed is high enough to sufficiently minimize the torque, and implicitly, the size of the electrical machine. The size of the electric machine is also reduced, since cooling is done with water. Power electronics are installed between the generator and the grid to allow for a variation of the rotational speed of the electrical machine and thus the turbine one. The power electronics are composed of two Emerson M700 frequency converters, one driving the generator, the other ensuring the current injection into the network. The rotational speed of the machine is the degree of freedom of the system to stay at the best efficiency point when the upstream flow velocity varies, thus keeping a constant tip speed ratio.

To assess the electrical performance on the test rig, the testing generator was first coupled with an entrainment motor equipped by an absolute encoder. A torque meter was mounted on the shaft between the two electrical machines, while an Emerson M700 frequency converter drives the entrainment motor. A Zimmer LMG 670 precision multimeter finally measured the output electrical values from the generator.

The performances of the gearbox were also measured. To perform the experiment, the generator and the gearbox were tested together; see Figure 5a. A specific system allows the manual breaking. A torque meter was inserted between the output of the gearbox and the manual break in order to measure the effective torque on the shaft. The signal of the torque meter and certain electrical values from the precision multimeter were synchronously acquired by a signals digitizer. The performance measurements are based on a synchronized dynamic acquisition of all sensors signals.

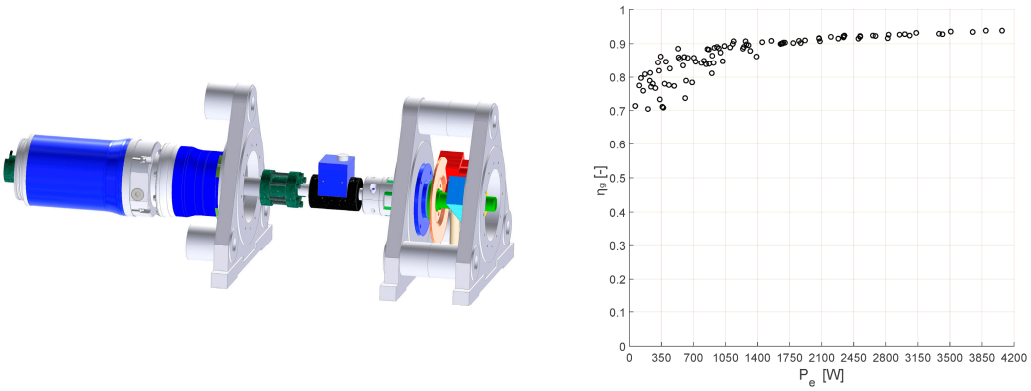

(**a**) (**b**)

Figure 5. (**a**) Assembly of the generator and gearbox in the laboratory, (**b**) efficiency of the Permanent Magnets Synchronous Motor generator.

Firstly, the efficiency of the generator was measured in Figure 5b. A maximal efficiency of about 93% was reached for the maximal power of the generator. In the operating range of the kinetic turbine power, those efficiencies were between 75% and 90%.

Then, the efficiency of the assembly generator gearbox was established as a function of the current at the terminals of the generator and the speed of the generator. The resulting hill chart, using all the dynamic measured points, is represented in Figure 6, remarking that the resulting torque is considered instead of the current of the generator. A maximum value of 88% was reached for the electro-mechanical efficiency η_{e-m} for a generator rotational speed of 683 min^{-1} and a torque of 260 N·m at the gearbox output. The full load and the nominal expected operating points specified in Table 1 are indicated respectively with a blue and a grey dot on the 2D electro-mechanical efficiency hill-chart.

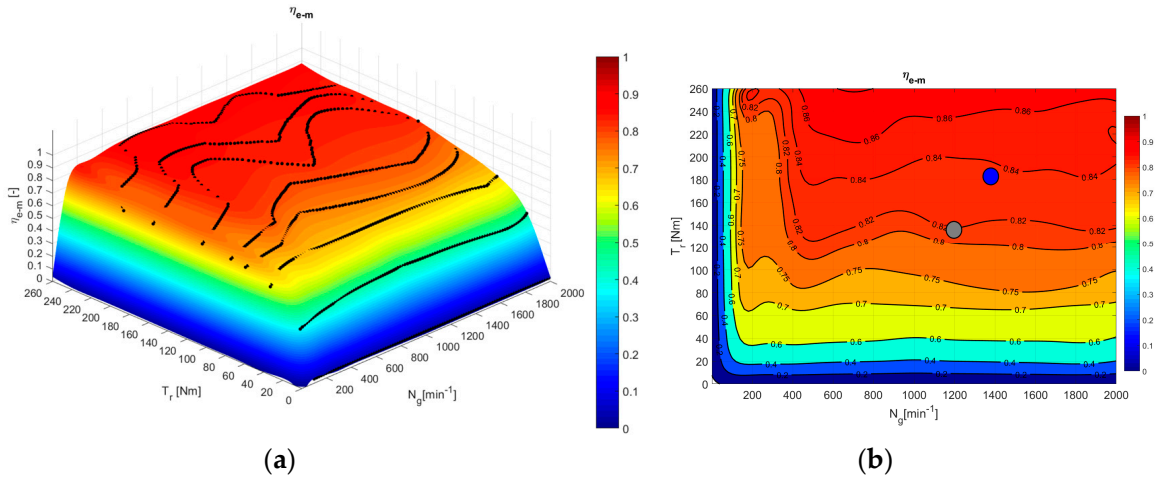

(**a**) (**b**)

Figure 6. (**a**) Resulting 3D and (**b**) 2D efficiency hill-charts of the kit gearbox—generator.

3.3. Identification of Variables on Site

On site, the following variables are monitored on the generator: (i) voltage at the terminals U_g; (ii) current at the terminals I_g; and (iii) rotational speed N_g. The electrical power P_e can then be calculated using U_g and I_g.

The mechanical–electrical efficiency η_{e-m} can be identified using the laboratory measurements N_g and the current I_g. The mechanical power P_m can thus be estimated.

The rotational speed of the runner N_r can also be calculated using the factor of 16, with the rotational speed of the generator N_g.

Another important value is also measured on site: the velocity of the upstream flow C_∞. This value allows us to calculate the tip speed ratio of the turbine; see Equation (2). The hydraulic power P_h and the power coefficient C_p can be estimated as well; see Equation (1). Finally, the behavior of the turbine can be completely described using the measurement on site and the variables identified in laboratory.

4. Pilot Site

4.1. General Description

The tailrace canal of the Lavey run-of-river power plant, installed in the western side of Switzerland on the Rhône River, was chosen as the pilot site to assess the hydraulic performances of the kinetic turbine prototype. Commissioned in 1950, the Lavey hydroelectric power plant is fed by an underground headrace gallery of 4 km length connected to the upstream run-of-river dam that ensures a maximum derived discharge of 220 m^3/s. The underground hydroelectric plant is equipped with three vertical-axis Kaplan turbines, which recover the hydraulic power from 34 m to 42 m head. The flow exits the draft tubes by three tailrace tunnels directly connected with the tailrace canal. The latest, as illustrated in Figure 7, presents a regular trapezoidal cross section over about 600 m before reaching again the natural course of the river. Finally, the open air testing platform was installed in the upstream side of the downstream bridge, an implantation location that ensures an optimal testing condition over the whole year independent of the power plant operating mode [17].

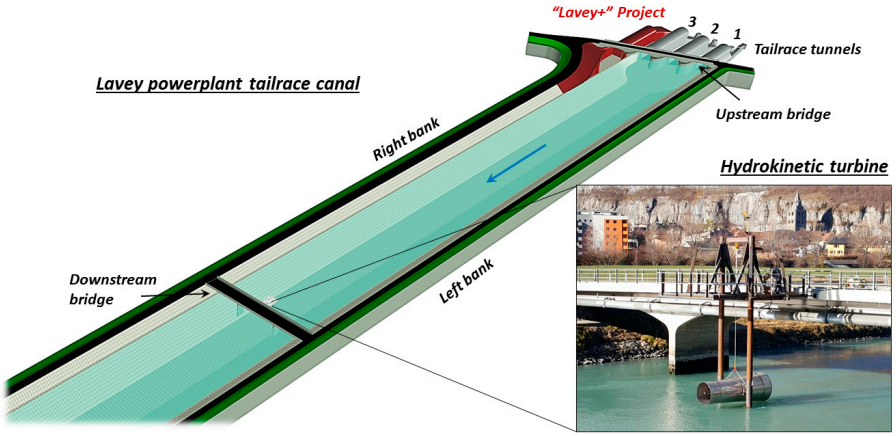

Figure 7. Tailrace canal of Lavey—full 3D CAD isometric view and photograph with the open-air platform installed in the canal toward the downstream bridge.

4.2. Flow Pattern

Prior to the installation of the testing platform, the kinetic potential of the tailrace canal was investigated under different operating conditions, with two and three operating turbines at once. The study included incompressible unsteady free-surface flow numerical simulations validated with experimental velocity measurements in three cross sections of the canal [17]. In the framework of the current testing campaign of the kinetic turbine, similar to the previous experimental tests, an ADCP system installed on a floating boat was employed to perform velocity measurements in different sections of the canal. According to the analysis of previous numerical simulations, the floating boat was installed 40 m from the kinetic turbine to measure the upstream flow velocity to avoid the influence of the machine. In Figure 8, the resulting 100 instantaneous axial velocity profiles in a mid-section of the canal upstream of the testing platform along with the time average values at each available water depth are provided. The period between two consecutive sets of instantaneous velocity measurements is of 1.33 s. Then, in the right plot, the axial velocity profiles in the same canal mid-span section along with the upstream distance show almost the same distribution with the water depth.

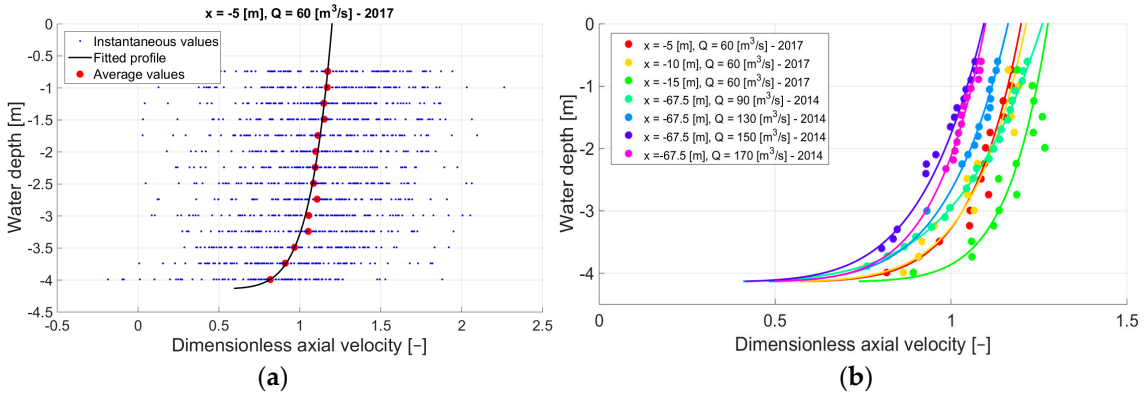

Figure 8. Resulting measured axial velocity profiles in the mid-span longitudinal section of the tailrace canal upstream of the testing platform: (**a**) instantaneous values, averages and fitted profile; (**b**) average and fitted profiles.

Considering that the velocity values are divided by the discharge velocity of the corresponding section, one may state here that the velocity profile in the span-wise direction is almost uniform for large discharge values, while for small discharge values, the main flow is organized in the center of the

canal. Indeed, for small discharge values, the axial velocity in the middle of the canal is much higher than the discharge velocity, which increases locally its kinetic potential.

5. Performance Measurements

The main objective of this project was to investigate experimentally the behavior of this new kinetic turbine. Due to the limited cross section of the artificial canals, it was quite challenging to predict the effect of free surface flow and the blockage effect using numerical simulation.

During the different campaigns, the discharge in the pilot canal site varied due to the natural discharge variation of the Rhône River and the operating conditions of the upstream run-off-river power plant, allowing us to explore the complete operating range of the machine. Moreover, the influences of the turbine depth and the tilt angle of the turbine axis were investigated.

To obtain the evolution curves of the power coefficient C_p as a function of the tip speed ratio based on the measurement points, some assumptions were considered. First, the noisy time signals of the ADCP were smoothed by means of a moving average low-pass filtering. Then, a space averaged time signal was calculated using the smoothed signals of three cells with a span-width of 0.25 m, around the turbine axis depth, corresponding to a total height of 0.75 m or in other words to 75% of the turbine runner diameter. Prior to this, a correlation with the measured discharge of the Lavey plant was used to eliminate all values during transient operating conditions of the power plant, only constant discharge periods being thus considered. Further, a variable time-shift vector (dependent on the measured velocity and on the downstream position of the machine regarding the position of the ADCP) was calculated to synchronize the measurements performed by the ADCP and the control/monitoring system of the machine. Finally, the upstream reference velocity C_∞ was calculated by a time-average of the previously obtained space-averaged signal using 10 samples (the time period between samples is 1.33 s).

5.1. Influence of the Depth

The maximal power coefficient and its corresponding tip speed ratio measured for a configuration with no tilt and a depth of 2.5 m are used as a reference to define the normalized power coefficient C_p^* and the normalized tip speed ratio λ^*. Figure 9 shows C_p^* as a function of λ^* for different depths: 1 m, 1.5 m, and 2.5 m at two different tilts respectively of 0 and 6 degrees. These graphs intend to demonstrate the impact of the implantation depth level.

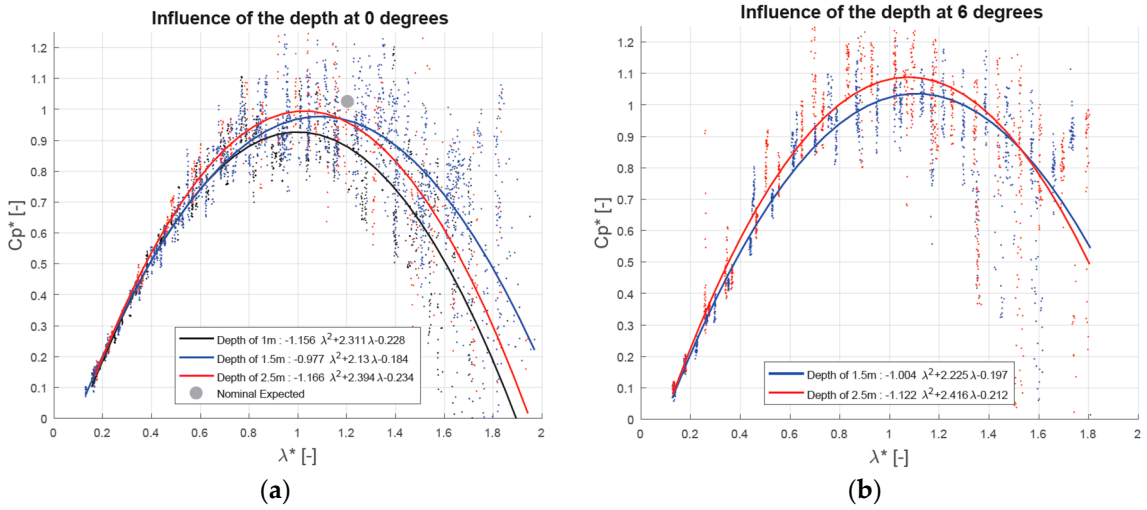

Figure 9. Power coefficient (**a**) for three depths of 1 m, 1.5 m and 2.5 m for a tilt of 0° and (**b**) for two depths 1.5 m and 2.5 m for a tilt of 6°.

The power coefficient C_p^* is expected to be higher close to the free surface according to the velocity profiles shape in a free-surface canal; see Figure 8. However, the experimental measurements demonstrate that the highest value of the C_p^* is reached at the depth of 2.5 m. An explanation of this result is that the platform base induces a local blockage effect, which increases the flow velocity in the turbine close to the canal bottom for the depth of 2.5 m. This effect is observed for the two-tilt angle considered in the figure. The maximum values of the power coefficient are reached for a normalized tip speed ratio between approximatively 1 and 1.2 to selected depth values not far from the nominal expected operating point indicated with a grey dot. It confirms the quality of the design development using numerical simulations; see [16].

The curve fitted on the measurements is based on a quadratic polynomial function for a tip speed ratio higher than 0.2. The part of the curve, which is not covered by the measurements for a lower tip speed ratio and which must pass through the origin, should be described by another equation. Off-design conditions are always difficult to measure with high precision, and the underlying physical phenomena developing at a low tip speed ratio seem to present a different asymptotic behavior.

Contour plots of the power coefficient as a function of the runner rotational speed and the upstream velocity are represented in Figure 10 for the three explored depths. The power coefficients are optimal for a rotation speed of the runner between 40 and 80 min^{-1}. For a depth of 1.5 m, the nominal rotational speed corresponds approximately to 70 min^{-1} and an upstream velocity of 1.5 $\text{m}\cdot\text{s}^{-1}$, which are in the range of the expected designed nominal operating conditions. The investigated range of the upstream velocity is higher for the depth of 1.5 m explaining the extended contour plot.

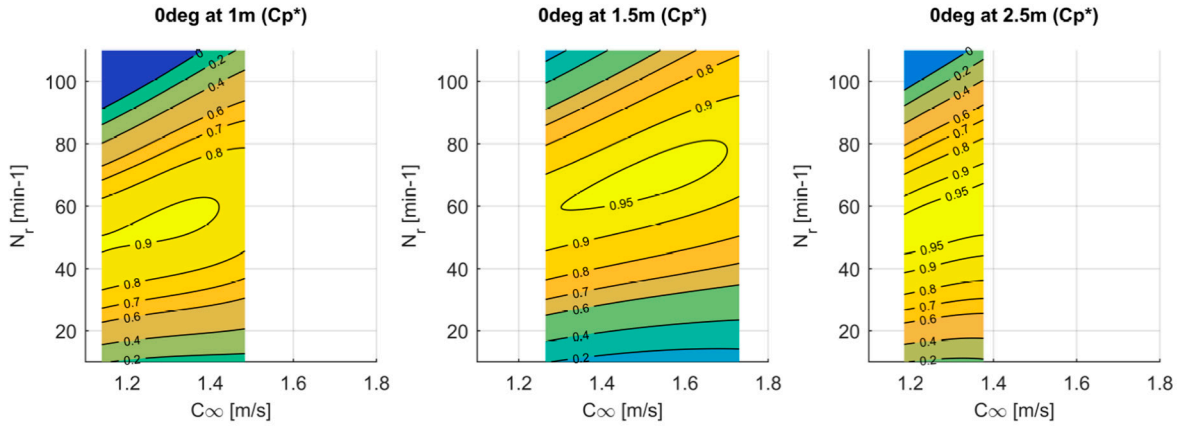

Figure 10. Power coefficient for a tilt of 0° for three depths: 1 m (**left**), 1.5 m (**middle**) and 2.5 m (**right**).

5.2. Influence of the Tilt

In Figure 11, the influence of the tilt of the machine axis is shown. The measurements were performed at different tilts: 0, 3, 6, and 10 degrees. The fitting curves are also based on a quadratic polynomial function for the explored tilt values.

The inclination of the machine improves its performance. An increase of 3% between 0 and 3 degrees is observed, while an increase of 6% is reached between 0 and 6 degrees for the tested depth of 1.5 m. At the depth of 2.5 m, the gaps are even more significant, with an increase reaching more than 12%. A maximum value is reached for a tilt of 10°. Unfortunately, a higher tilt cannot be reached with the current facility. Further numerical simulations could be used to identify the critical tilt value when the power coefficient will decrease again.

To explain the improvement of the power coefficient, one of the key factors is the global blockage effect of the turbine in the canal. Indeed, at no tilt, the blockage ratio B, defined as the ratio between the frontal area of the immerged part of the platform with the turbine and the canal area Ac, is estimated to be 5.85%. At 10°, the blockage ratio reaches the value of 6.22%. Those values are lower than 10%, which means that the blockage effect is limited [20]. Nevertheless, a relative increase of this ratio of

more than 6% can explain the increase of the power coefficient. An increase of the blockage ratio causes a larger local deformation of the free surface above the turbine, the energy harnessed by the turbine representing a loss for the free surface flow. It means an increase of the available hydraulic energy available between the inlet and the outlet of the turbine. At no tilt, the hydraulic energy available for the turbine is mainly the kinetic energy of the flow going into the machine and crossing the runner. When the turbine axis is inclined, the potential energy difference between the inlet and the outlet sections induced by the blockage effect participates in the available hydraulic energy for the turbine and thus a higher power coefficient is reached. A widening of the range of the λ^*, where the C_p^* values are high and there is a displacement of the optimal value of λ^* with the tilt, is also observed as perceived by Kolekar and Banerjee [20]. At 2.5 m depth, the nominal tip speed ratio seems to increase with the tilt but at 6 degrees a non-expected lower value is observed.

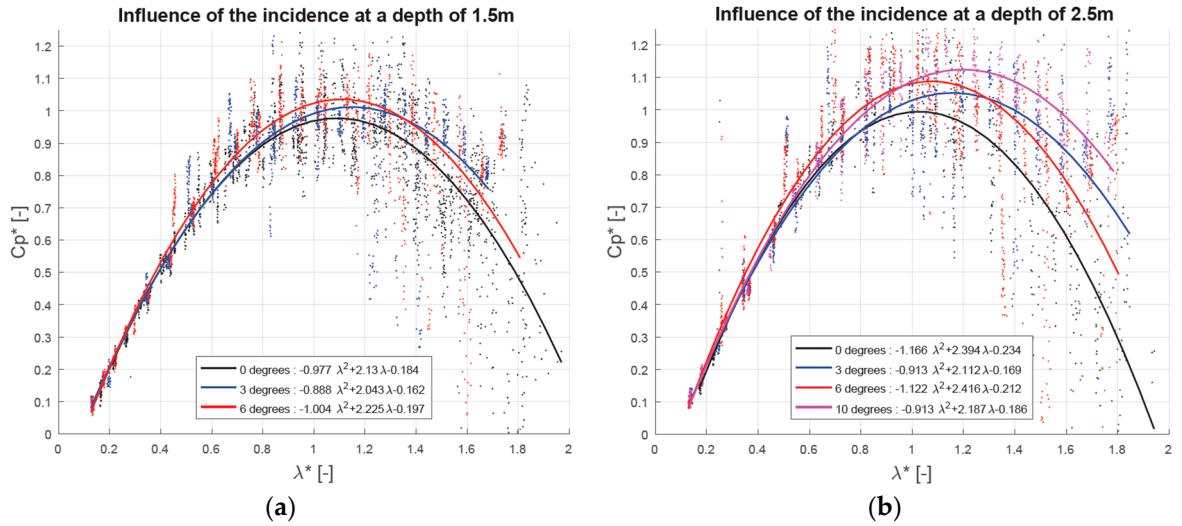

Figure 11. Power coefficient for different tilts from 0 to 10 degrees, for two depths (**a**) 1.5 m and (**b**) 2.5 m.

In Figure 12, contour-plots of the power coefficient are represented as a function of the runner rotational speed and the upstream velocity for two depths 1.5 m and 2.5 m and three tilts 0°, 3°, and 6°. There are not enough measurements at 10° to obtain well-defined contour-plots.

At 1.5 m depth, the peak of the hill chart can be found for an upstream velocity from 1.2 m·s^{-1} to 1.6 m·s^{-1}. The nominal rotational speed of the runner stays in the range of 40 min^{-1} to 80 min^{-1}.

A maximum value of C_p^* is reached for 6° at 2.5 m. At this depth, the influence of the tilt is more visible. The hill-chart peak even seems to move to lower rotational speed and higher upstream flow velocity while the tilt increases, which means a lower tip speed ratio. This observation can be made also in Figure 11 at 6°. Nevertheless, this trend will reverse at 10° according to Figure 11.

Globally, the area where the power coefficient is high becomes larger, while the tilt increases for both depths. This result can be very interesting for the industrialization phase of the project. Indeed, a final solution without the variable rotational speed could be considered to decrease the cost of the product. A tilt of the turbine axis should then allow for maintaining a larger operating range of the upstream velocity at a high power coefficient.

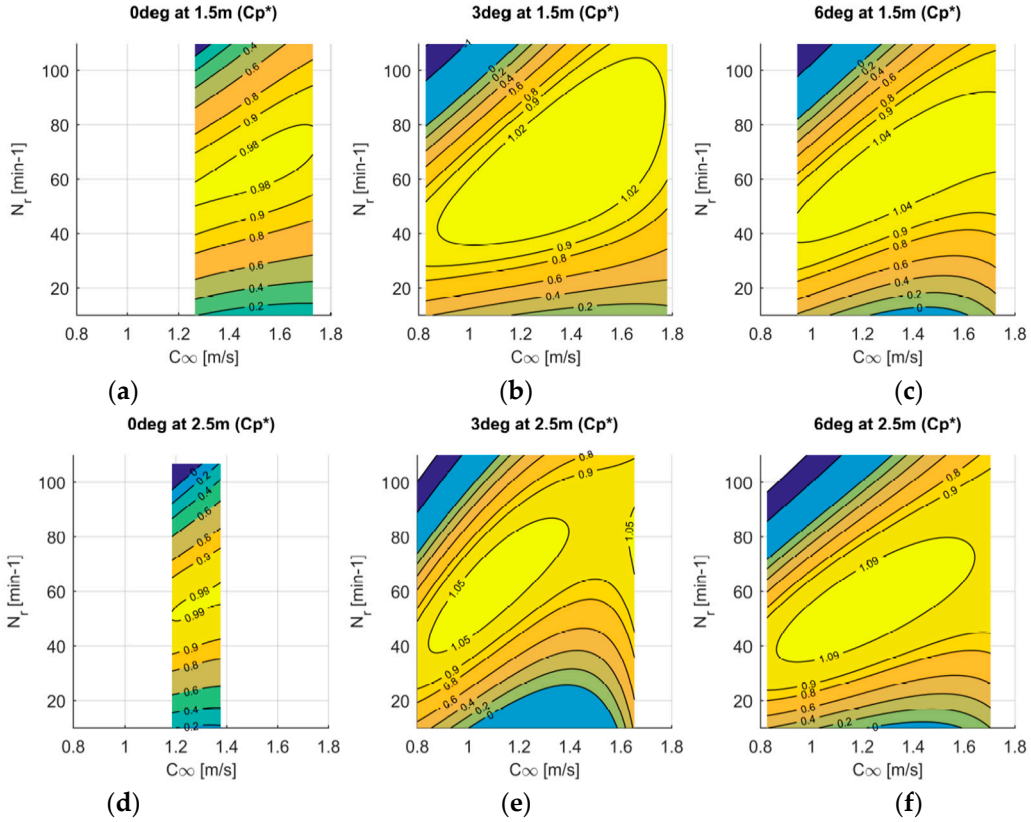

Figure 12. Power coefficient as a function of the tip speed ratio for different tilts and depths : (**a**) for 0° and 1.5 m depth, (**b**) for 3° and 1.5 m, (**c**) for 6° and 1.5 m, (**d**) for 0° and 2.5 m, (**e**) for 3° and 2.5 m depth and (**f**) for 6° and 2.5 m depth.

5.3. Nominal Conditions of the Kinetic Turbine

Tables 3 and 4 summarize the optimal values for the power coefficient and the tip speed ratio during the measurement series.

Table 3. Optimal tip speed ratio.

Optimal ˘*			
depth	1 m	1.5 m	2.5 m
0 degrees	0.97	1.11	1
3 degrees	-	1.17	1.16
6 degrees	-	1.08	1.08
10 degrees	-	-	1.18

Table 4. Optimal power coefficient.

Optimal C_p*			
depth	1 m	1.5 m	2.5 m
0 degrees	0.93	0.98	1
3 degrees	-	1.02	1.05
6 degrees	-	1.04	1.09
10 degrees	-	-	1.12

As a reminder, the expected values from the design phase are respectively 2.65 and 0.85 for the nominal tip speed ratio λ and power coefficient C_p (see Table 1), corresponding respectively to 1.20 for

λ^* and 1.02 for $C_p{}^*$ using the normalization with the reference case. It can be observed that the target value for the power coefficient was reached and even exceeded for the performances using the tilt effect. The influence of the depth was not expected, since the power coefficient is higher close to the bottom of the canal. One explanation is the effect of the platform base, which creates a local blockage effect of the flow and thus increases the flow velocity inside the turbine. It has to be confirmed with further investigations using the numerical simulation. The influence of the tilt angle can be clearly observed in Table 4 for each investigated depth. It can be explained by the increase of the global blockage effect. This result has also been confirmed using numerical simulation. Finally, the higher value for the power coefficient is reached for a tilt of 10 degrees and a depth of 2.5 m. For those conditions, the power coefficient is equal to 0.93 or 1.12 using the normalization with the reference case.

6. Conclusions

The present paper presents an experimental investigation of the performance of a first prototype of a kinetic turbine installed in a tailrace canal of a run-of-the-river power plant in Switzerland. This kinetic turbine was first developed using numerical simulations and this experimental phase is a crucial step to assess the previous development. An experimental procedure including laboratory and on-site tests was set up to measure the power coefficient of the turbine as a function of the tip speed ratio. The measured values correspond to the expected performance according to the design phase: values of the power coefficient between 0.77 and 0.93 were measured for a tip speed ratio between 2.1 and 2.6. The influence of two parameters was explored: the depth of the turbine axis compared to the free surface and the tilt of the turbine axis compared to a standard horizontal position. The performance of the turbine increases with the depth and the tilt; indeed, the higher power coefficient was measured for the larger depth and tilt investigated. The interpretations of the observed influences of those parameters are the local blockage effect of the platform base for the depth and the global blockage effect of the platform with the turbine in the artificial channel. Those explanations need to be confirmed by further numerical investigations.

Acknowledgments: The present study was carried out in the framework of a Pilot & Demonstrator Project financially supported by the Swiss Federal Office of Energy, The Ark Foundation for Innovation in Valais, Switzerland and the Swiss Competence Center for Energy Research—Supply of Electricity. The authors would like to express a special thanks to the "Services Industriels de Lausanne" and "Usine de Lavey" industrial partners for their approval and technical support in using the tailrace canal of the Lavey power plant and Swiss-SIT for their support in the risk analysis of this project.

Author Contributions: All the authors have contributed in writing the paper. Cécile Münch-Alligné, Jérémy Schmid, Sylvain Richard, Anthony Gaspoz and Vlad Hasmatuchi set up the experiments and performed the analysis presented here with the help of Stahleinbau GmBH represented by Nino Brunner who manufactured the turbine and the platform.

Conflicts of Interest: The authors declare no conflict of interest.

Nomenclature

Symbols

Ac	[m^2]	Canal Area of the test section: 137 m^2.
C_p	[-]	Power coefficient.
$C_{p\,ref}$	[-]	Maximal power coefficient at no tilt and a depth of 2.5 m equal to 0.83.
C_∞	[$m{\cdot}s^{-1}$]	Upstream reference flow velocity.
I_g	[A]	Current at the generator terminals.
N_g	[min^{-1}]	Rotational speed of the generator.
N_r	[min^{-1}]	Rotational speed of the runner.
P_e	[W]	Electrical power.
P_h	[W]	Hydraulic power.
P_m	[W]	Mechanical power.

Q	[$m^3 \cdot s^{-1}$]	Discharge.
R^*	[m]	Hub-to-shroud normalized radius
R_r	[m]	Runner outer radius.
T^*_{CFD}	[N·m]	Cumulated runner torque predicted by CFD normalized by the total torque.
T_r	[N·m]	Torque at the runner shaft.
U_g	[V]	Generator output voltage.
x	[m]	Upstream longitudinal distance.
η_g	[-]	Generator efficiency.
$\eta_{e\text{-}m}$	[-]	Electro-mechanical efficiency.
λ	[-]	Tip speed ratio.
λ_{ref}	[-]	Tip speed ratio equal to 2.2 corresponding to $C_{p\ ref.}$
ρ	[$kg \cdot m^{-3}$]	Water density
ω_g	[$rad \cdot s^{-1}$]	Angular speed of the generator
ω_r	[$rad \cdot s^{-1}$]	Angular speed of the runner

Abbreviations

ADCP	Acoustic Doppler Current Profiler
PMSM	Permanent Magnet Synchronous Motor

References

1. US Department of Energy, Energy Efficiency and Renewable Energy. *Wind and Hydropower Technologies, Feasibility Assessment of the Water Energy Resources of the United States for New Low Power and Small Hydro Classes of Hydroelectric Plants*; Tech. Rep. DOE-ID-11263; Idaho Operations Office: Washington, DC, USA, 2006.
2. Khan, A.M.J.; Bhuyan, G.; Iqbal, M.T.; Quaicoe, J.E. Hydrokinetic energy conversion system and assessment of horizontal and vertical axis turbines for river and tidal applications: A technology status review. *Appl. Energy* **2009**, *86*, 1823–1835. [CrossRef]
3. Yuce, M.I.; Muratoglu, A. Hydrokinetic energy conversion systems: A technology status review. *Renew. Sustain. Energy Rev.* **2015**, *43*, 72–82. [CrossRef]
4. Verdant Power, LLC, 4640 13th Street, North, Arlington, VA 22207, USA. October 2008. Available online: http://www.verdantpower.com/kinetic-hydropower-system.html (accessed on 12 March 2018).
5. Ruopp, A.; Ruprecht, A.; Riedelbauch, S.; Arnaud, G.; Hamad, I. Development of a hydro kinetic river turbine with simulation and operational measurements results in comparison. In *IOP Conf. Series: Earth and Environmental Science*; IOP Publishing: Bristol, UK, 2014; Volume 22, p. 062002.
6. Bertrand, O.; Duron, L.; Girard, C.; Zanette, J.; Dominguez, F. Numerical modelling of vertical-axis and transverse-flow hydrokinetic turbine in the river Loire. In Proceedings of the 36th IAHR World Congress, The Hague, The Netherlands, 28 June–3 July 2015.
7. Betz, A. Das Maximum der theorish möglichen Ausnutzung des Windes durch Windrotoren. *Zeitschrift für das gesamte Turbinewesen* **1920**, *26*, 307–309.
8. Igra, O. Research and development for shrouded wind turbine. *Energy Convers. Manag.* **1981**, *21*, 13–48. [CrossRef]
9. Kirke, B. *Development in Ducted Water Current Turbines*; Tidal Paper; School of Engineering, Griffith University: Nathan, Australia, 2003; pp. 1–12.
10. Lawn, C.J. Optimization of the power output from ducted turbines. *Part A J. Power Energy* **2003**, *217*, 107–117. [CrossRef]
11. Luquet, R.; Bellevre, D.; Fréchou, D.; Perdon, P.; Guinard, P. Design and model testing of an optimized ducted marine current turbine. *Int. J. Mar. Energy* **2013**, *2*, 61–80. [CrossRef]
12. Laurens, J.-M.; Ait-Mohammed, M.; Tarfaoui, M. Design of bare and ducted axial marine current turbines. *Renew. Energy* **2016**, *89*, 181–187. [CrossRef]
13. Official Website of the Swiss Federal Office for Energy. Available online: http://www.bfe.admin.ch (accessed on 12 March 2018).
14. *Le Potentiel Hydroélectrique de la Suisse*; Swiss Federal Office for Energy (SFOE): Bern, Switzerland, 2012.

15. Biner, D.; Hasmatuchi, V.; Violante, D.; Richard, S.; Chevailler, S.; Andolfatto, L.; Avellan, F.; Münch, C. Engineering & Performance of DuoTurbo: Microturbine with Counter-Rotating Runners. In *IOP Conference Series: Earth and Environmental Science*; IOP Publishing: Bristol, UK, 2016; Volume 49, p. 102013.
16. Münch-Alligné, C.; Gaspoz, A.; Richard, S.; Hasmatuchi, V.; Brunner, N. New prototype of a kinetic turbine for artificial channels. In *Advances in Hydroinformatics*; Springer: Singapore, 2018; pp. 981–996.
17. Hasmatuchi, V.; Avellan, F.; Münch, C. Numerical Modelling of a Run-of-River Tailrace Channel. In Proceedings of the Hydro 2014, Cernobbio, Italy, 13–15 October 2014.
18. Hasmatuchi, V.; Alligné, S.; Kueny, J.-L.; Münch, C. Hydraulic performance of a new isokinetic turbine for rivers and artificial channels. In Proceedings of the 36th IAHR World Congress, The Hague, The Netherlands, 28 June–3 July 2015.
19. Williams, H.L. Tidal Flow Hydroelectric Turbine. U.S. Patent 7,378,750 B2, 27 May 2008.
20. Kolekar, N.; Banerjee, A. Performance characterization and placement of a marine hydrokinetic turbine in a tidal channel under boundary proximity and blockage effects. *Appl. Energy* **2015**, *148*, 121–133. [CrossRef]